Chapter 2

Novel Ionic Mesogenic PyTp and ImTp Molecules at Air-Water and Air-Solid Interfaces

2.1 Introduction

The studies on discotic molecules at air-water (A-W) and air-solid (A-S) interfaces have drawn lot of attention [1, 2]. The thin films of discotic mesogens have technological applications in the fabrication of gas sensors [3], field-effect transistors [4], photovoltaic diodes [5], solar cells and optical displays [6]. In addition, these systems have scientific interest in modeling of Π-Π and steric interactions in two-dimensional and biological systems [7]. Disk-like molecules, like porphyrins, vitamins and so on, play significant role in living systems as well.

At A-W interface, discotic mesogens can self-assemble into one-dimensional columnar superstructures due to the overlapping of Π-orbitals of adjacent molecules and can arrange in a two-dimensional lattice, thereby forming stable Langmuir monolayers [2, 8]. These films need to be transferred to solid supports for practical applications. The preparation of ultra thin films by means of Langmuir-Blodgett (LB) technique is an efficient method to obtain highly ordered layers over large areas [9]. LB technique has the advantage of both macroscopical and microscopical influence on the molecular arrangement by means of the surface pressure variations and interactions with the aqueous subphase. LB films of discotic mesogens have been reported to have a surface morphology which are periodically modulated by columns that lie predominantly along the film deposition direction [1]. Evidence has been presented for square-lattice discotic structure in the bilayer films

obtained by LB technique [10]. Ionov et al. have experimentally established, smectic-like structure normal to the substrate, and the nematic-like in plane arrangement of the discotic molecules in the LB films [11], resembling a discotic smectic-nematic phase [12]. The possibilities to induce different structural arrangement in the LB films of discotic molecules allow to undertake detailed studies of the intra and interlayer molecular interactions, and especially of the steric and Π-Π interactions. With discotic mesogens, the effects of Π-Π and steric interactions on the LB film structure are stronger as compared to the case of the classical rod-like amphiphiles. These interactions also govern the structure and properties of many biological disk-shaped aromatic molecules [13].

As compared to the conventional discotic liquid crystals, ionic discogens differ significantly as they combine the properties of liquid crystals and ionic liquids. This makes them promising candidates to design anisotropic ion-conductive materials because of the anisotropic structural organization and the presence of ions as charge carriers [14]. The long alkyl chains of mesogenic molecule act as an insulating sheet for the ion conductive channel. Yoshio et al. have reported one-dimensional ion transport in self organized columnar ionic liquids [15].

Although discotic molecules of alkoxytriphenylene derivatives have been reported to form stable Langmuir monolayers [16], there have been no reports on ionic alkoxytriphenylene derivative monolayers. In this chapter, we present the studies on Langmuir and LB films of novel cationic discotic molecules, *viz.*, pyridinium tethered with hexaalkoxytriphenylene with bromide counter-ion (PyTp) and imidazolium tethered with hexaalkoxytriphenylene with bromide counter-ion (ImTp). We find that both the molecules form stable monolayer. Interestingly, the surface pressure-area per molecule (π-A_m) isotherm was completely reversible. The LB films of PyTp with two layers showed patterns with regular rectangular voids elongated in the film deposition direction, whereas, the LB films of ImTp with two layers exhibited irregular shaped voids throughout the film.

2.2 Experiment

The materials PyTp and ImTp were synthesized in the chemistry laboratory of our institute by Prof. Sandeep Kumar and Santanu Kumar Pal [17, 18]. The compounds were purified by repeated recrystallizations with diethyl ether and characterized by ^{1}H NMR, ^{13}C NMR, IR, UV spectroscopy

and elemental analysis which indicated high purity (99%) of the materials. The thermotropic liquid crystalline properties of these materials were investigated by polarizing optical microscopy, differential scanning calorimetry and small angle X-ray diffraction (XRD).

The surface manometry experiments were carried out in a LB trough. The subphase used was ultrapure deionized water (pH 5.8) obtained from Millipore Milli-Q system. The materials were dissolved in chloroform (HPLC-grade) and stock solutions of 0.236 mM concentration were prepared. The stock solution was spread on the subphase drop by drop using a micro syringe (Hamilton). After spreading, the film was left for 20 minutes allowing the solvent to evaporate. The π-A_m isotherms were obtained by symmetric compression of the barriers with a constant compression rate of 0.103 nm^2/molecule/min. The equilibrium spreading pressure (ESP) was measured at a constant area of 100 cm^2. High humidity of the order of 92 ± 5% was maintained during the experiment to prevent any evaporation. To determine the ESP value, we monitored the π with time until the π value reached a saturation. Brewster angle microscopy (BAM) was carried out to observe the films at the A-W interface.

LB technique was employed to transfer various layers of the films onto hydrophilic and hydrophobic substrates at different target surface pressures (π_t) with a dipping speed of 2 mm/min. To obtain hydrophilic surfaces, we treated polished silicon wafers for about 5 minutes in hot piranha solution (mixture of conc. H_2SO_4 and H_2O_2 in 3:1 ratio) then rinsed in ultrapure deionized water and later dried. For hydrophobic surfaces, freshly prepared hydrophilic silicon substrates were dipped in hexamethyldisilazane (HMDS) for 12 hours then rinsed with HPLC grade chloroform.

Since LB technique is not very efficient at low surface pressure, we have used horizontal transfer technique to deposit films on substrates at low π. In this technique, the hydrophilic substrates were placed below the water surface in the Langmuir trough and then the monolayer was spread on the water surface. After compressing the monolayer to the target surface pressure, water was slowly drained out using a narrow glass capillary. This enabled the monolayer to slowly settle on the substrate as the water level was lowered. We have shown the schematic diagram of the horizontal transfer technique in Figure 2.1. This technique works well at all surface pressures. Unlike

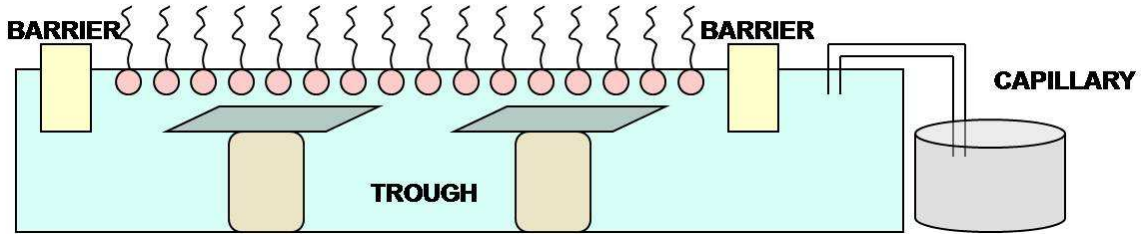

Figure 2.1: Schematic diagram of the horizontal deposition technique. This technique facilitates the deposition of Langmuir monolayer on hydrophilic substrates at low surface pressure where LB technique is not very efficient.

LB technique, only one layer can be deposited on a hydrophilic substrate using this method.

The atomic force microscope (AFM) studies on these films, obtained by both LB and horizontal techniques, were performed to study the film morphology and topography. We used silicon tips with spring constant of 21 N/m and resonance frequency of 250 kHz. The AFM images were acquired using the AC mode in ambient condition. All the images are shown without any image processing except flattening. UV-visible absorption spectroscopy was also carried out for the LB films transferred on quartz plate. All the experiments were carried out at room temperature (25 ± 0.5°C). The details of the experimental techniques are discussed in Chapter 1.

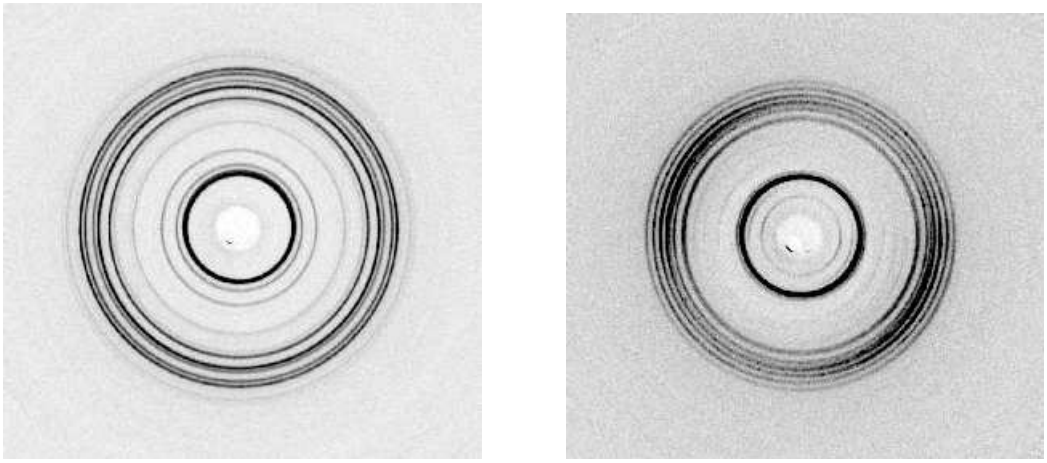

(a) PyTp (b) ImTp

Figure 2.2: X-ray diffraction patterns obtained for the materials PyTp and ImTp in the columnar mesophase at 85^0C.

2.3 Results

The material PyTp exhibits liquid crystalline phase in the bulk. It has the following phase sequence: Solid (S) – columnar phase (Col); 83.7°C, Col – isotropic (I); 95°C. On cooling, the columnar mesophase appeared at 92°C and remained stable down to room temperature [17]. The structure of the columnar mesophase obtained by small angle XRD (Figure 2.2(a)) reveals a simple rectangular lattice of parameter a = 4.24 nm and b = 3.64 nm. The material ImTp in the bulk also exhibits liquid crystalline phase and has similar phase sequence: S – Col; 67°C, Col – I; 101°C. On cooling, the columnar mesophase appeared at 98°C with the mesophase solidifying at 38°C [18]. The columnar phase has simple rectangular lattice with parameters a = 5.76 nm and b = 4.40 nm (Figure 2.2(b)).

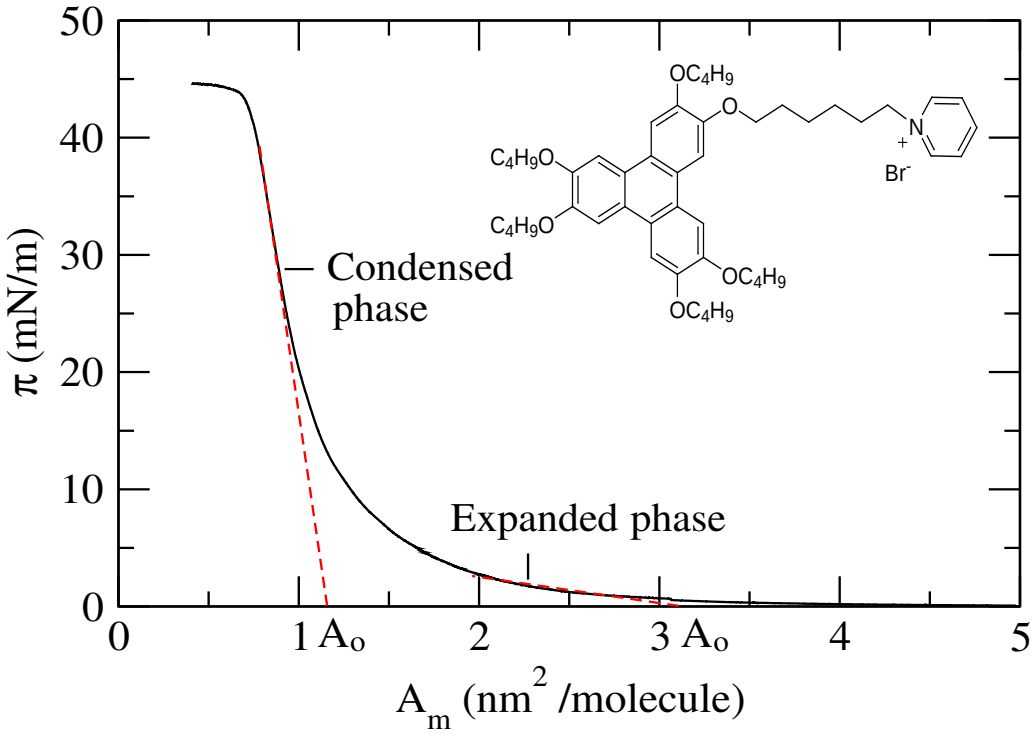

Figure 2.3: Surface pressure (π) - area per molecule (A_m) isotherm of pyridinium based discotic (PyTp) molecule. The extrapolation to zero surface pressure, shown by dashed lines, gives the limiting area per molecule A_o.

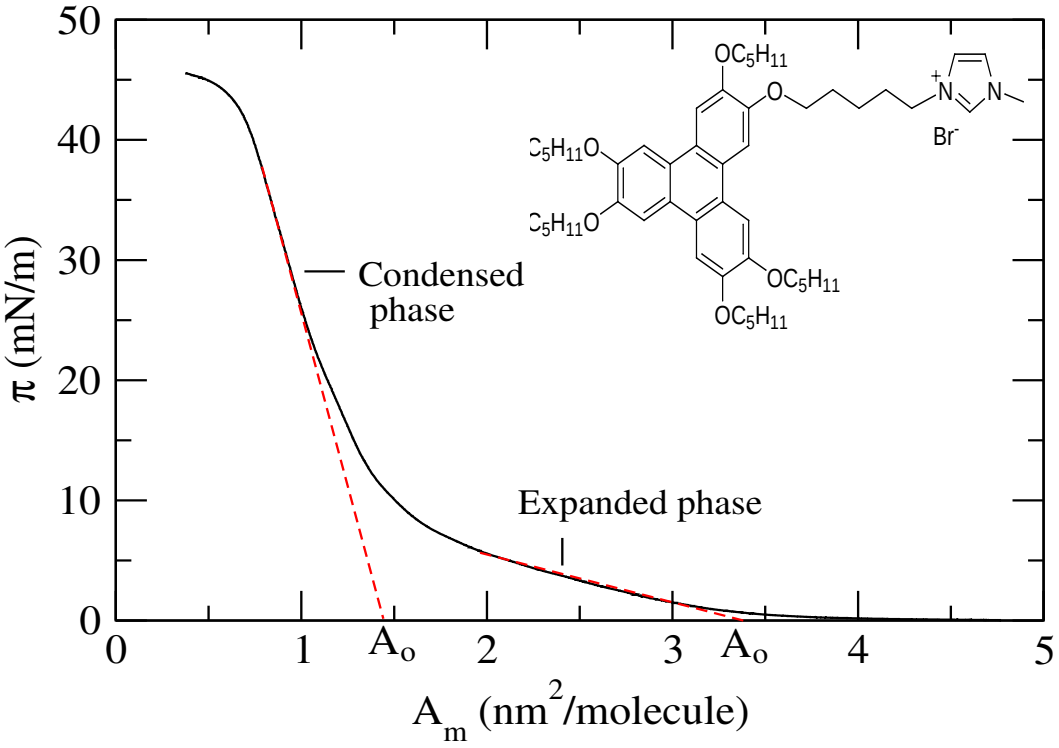

Figure 2.4: Surface pressure (π) - area per molecule (A_m) isotherm of imidazolium based discotic (ImTp) molecule. The extrapolation to zero surface pressure, shown by dashed lines, gives the limiting area per molecule A_o.

2.3.1 Surface Manometry

The surface pressure (π) - area per molecule (A_m) isotherms for PyTp monolayer and ImTp monolayer are shown in Figures 2.3 and 2.4 respectively. We find that, for both the films, there is a gradual rise in π up to 9 mN/m followed by a sharp rise. Both the isotherms exhibit a collapse pressure of about 44 mN/m. The limiting area per molecule (A_o) values obtained by extrapolation to zero surface pressure were 1.15 and 1.40 nm^2/molecule at the steep increasing region and 3.1 and 3.4 nm^2/molecule at the gradual increasing region, for the PyTp and the ImTp monolayers respectively. The rigidity of the films were calculated from the compressional elastic modulus $|E|$ given by

$$|E| = A_m \left(\frac{d\pi}{dA_m} \right) \tag{2.1}$$

The variation of $|E|$ with A_m for PyTp and ImTp monolayers are shown in Figure 2.5. The $|E|$ value showed a maximum of 83 mN/m at A_m of 0.871 nm^2/molecule for PyTp monolayer. The maximum value of $|E|$ for ImTp monolayer was 53.9 mN/m at A_m of 0.977 nm^2/molecule. We find a sharp change in the values of $|E|$ indicating a phase transition at an A_m of 1.6 nm^2/molecule for PyTp monolayer and at an A_m of 1.8 nm^2/molecule for ImTp monolayer. The phase below these A_m has much higher value of $|E|$ compared to the phase above these A_m values [19].

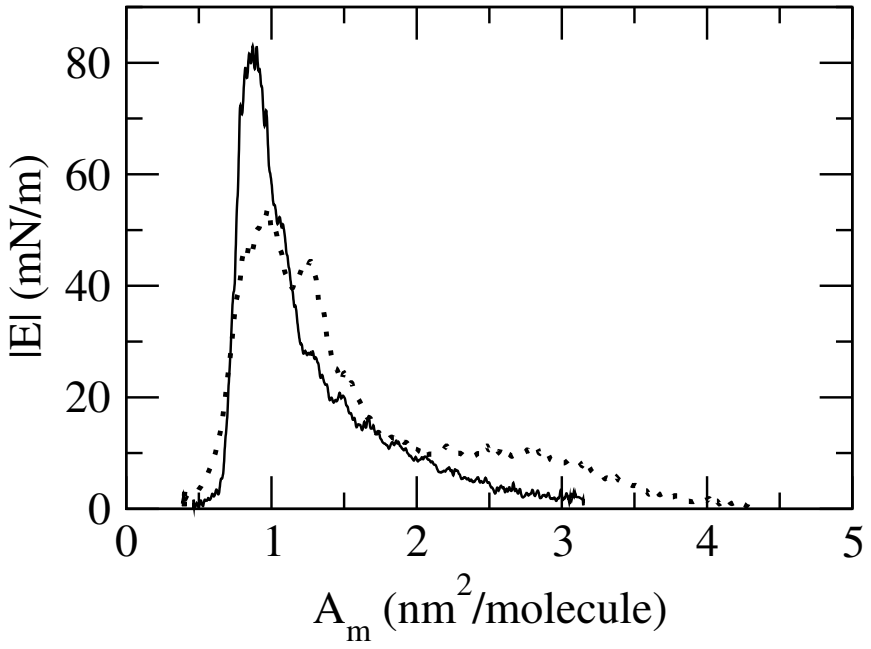

Figure 2.5: Variation of compressional elastic modulus (|E|) with area per molecule (A_m) for PyTp (continuous line) and ImTp (dotted line) monolayers.

The ESPs of PyTp and ImTp molecules were found to be around 9 mN/m (Figure 2.6). The time scale for the molecules to elude from the crystallites was of the order of a few seconds. The compression and expansion isotherm cycles for PyTp is shown in Figure 2.7. A negligible hysteresis was observed for the repeated compression and expansion of the isotherm over several cycles. Similar behavior was also observed for the ImTp isotherm cycles.

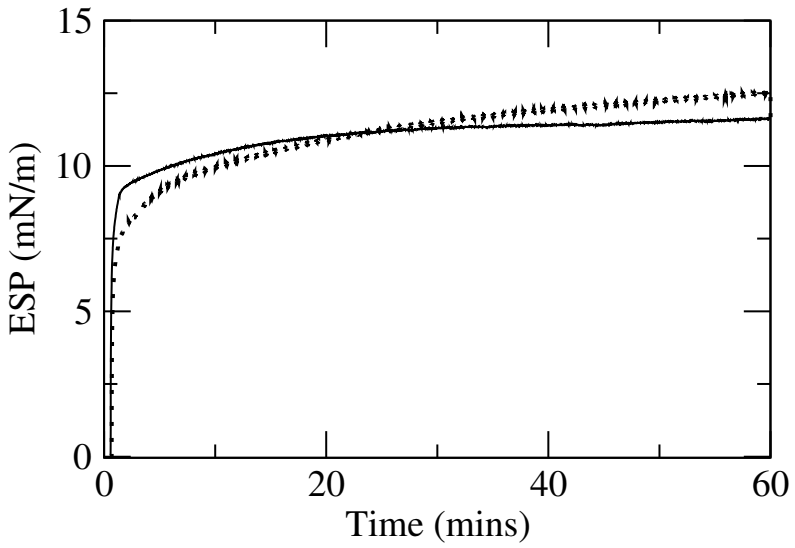

Figure 2.6: Equilibrium spreading pressure (ESP) of PyTp (continuous line) and ImTp (dotted line) molecules.

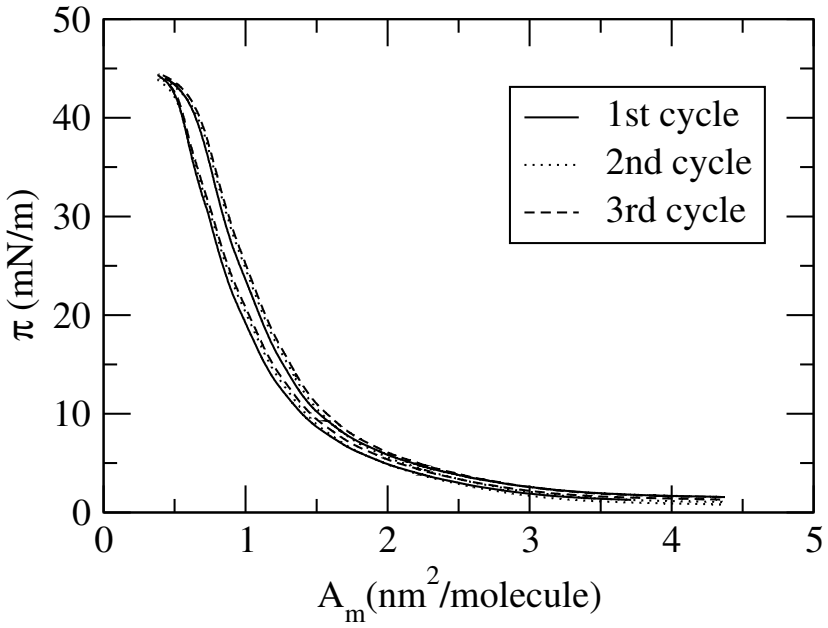

Figure 2.7: The π - A_m isotherm of PyTp showing reversibility from the collapsed state to the monolayer state with negligible hysteresis in the compression and expansion cycles.

2.3.2 Brewster angle microscopy

The monolayers of both PyTp and ImTp molecules were observed under BAM while performing the respective isotherms. Figure 2.8 shows the BAM images for the PyTp monolayer at various area per molecule. The BAM images show that the brightness increases gradually (Figure 2.8(b)) upon compression from nearly zero surface pressure (Figure 2.8(a)). This transforms to 3D crystals (Figure 2.8(c) and 2.8(d)) at the collapsed state. On expansion, these 3D crystalline domains disappeared and the system reverted back to the uniform intensity region indicating a monolayer state. Similar behavior was also observed for the ImTp monolayer.

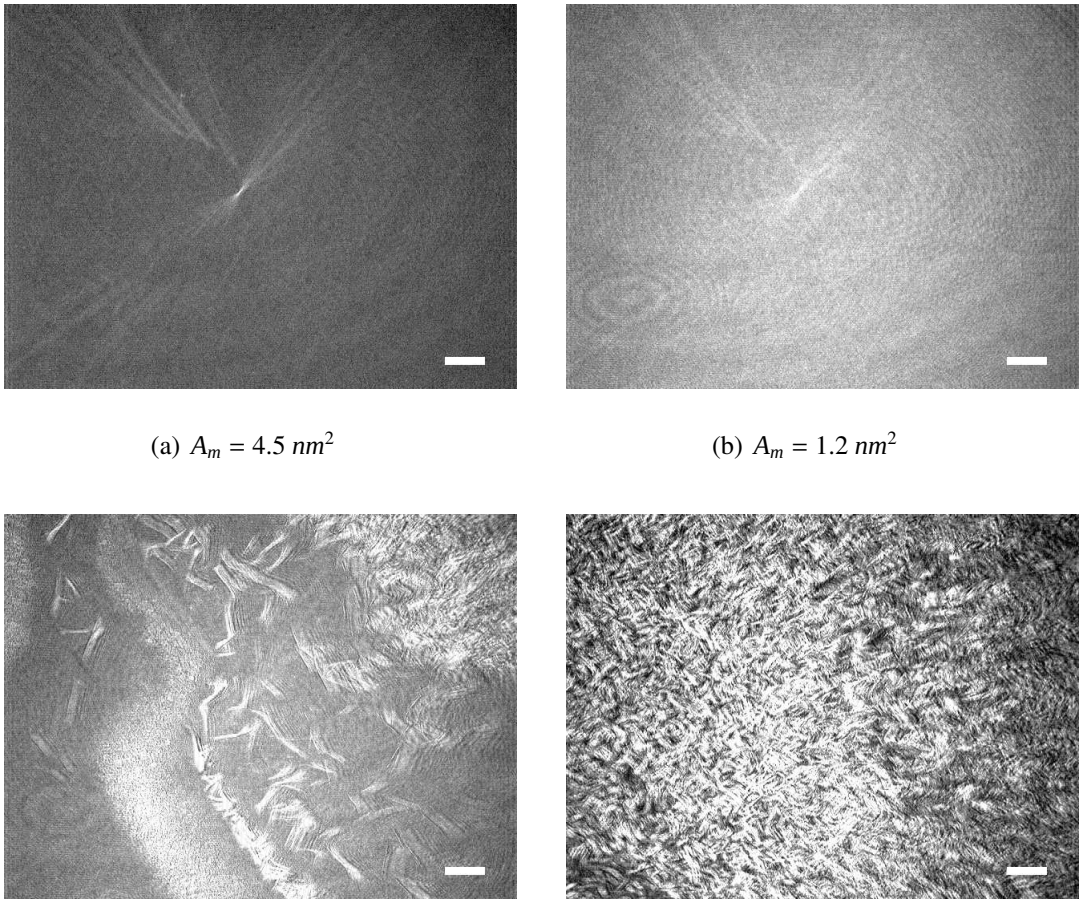

(a) $A_m = 4.5\ nm^2$ (b) $A_m = 1.2\ nm^2$

(c) $A_m = 0.7\ nm^2$ (d) $A_m = 0.35\ nm^2$

Figure 2.8: Brewster angle microscope images of PyTp monolayer for various area per molecule at air-water interface obtained on compressing the monolayer: (a) Expanded phase. (b) Condensed phase. (c) Coexistence of condensed phase and 3D crystals. (d) Collapsed state. The scale bar in each image represents 500 μm.

In addition, the spreading behavior of the systems were observed under BAM during ESP measurements. Figure 2.9 shows the BAM images taken at various time interval after placing a speck of crystallite of PyTp on the water surface. The molecules elude out from the bulk crystallites almost instantaneously and formed a monolayer at the A-W interface spontaneously (Figure 2.9(a)). In about 40 secs, the system reached an equilibrium state (Figure 2.9(b)) where the rate of elution of molecules from crystallites was equal to the rate of molecules binding to the crystallites.

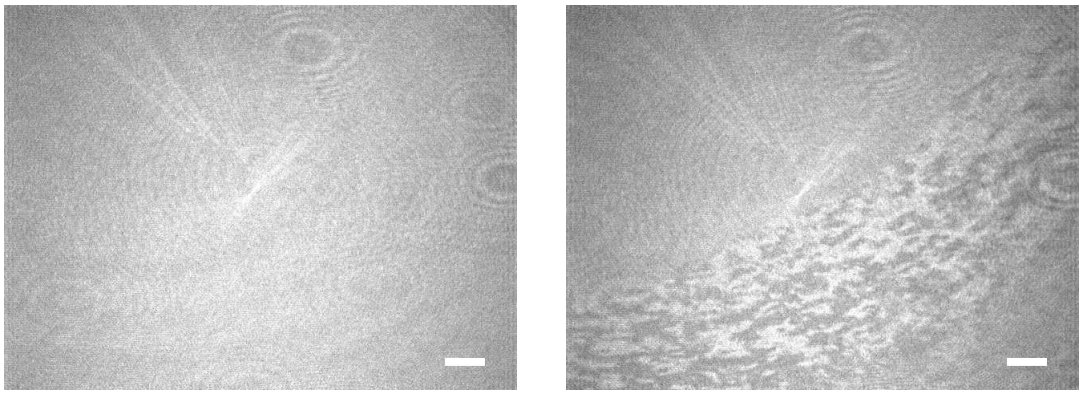

(a) 10 seconds (b) 40 seconds

Figure 2.9: Brewster angle microscope images at (a) 10 seconds, and (b) 40 seconds showing the fast spreading of the PyTp molecules at the A-W interface. The scale bar in each image represents 500 μm.

2.3.3 Atomic Force Microscopy

The AFM topography of the ImTp monolayer transferred by horizontal method on hydrophilic silicon substrate at a target surface pressure of 5 mN/m is shown in Figure 2.10(a). The height profile of the image shows the height of the film to be 0.7 nm with reference to the substrate. The films transferred by LB technique at target surface pressures of 35 mN/m and 45 mN/m are shown in Figures 2.10(b) and 2.10(c) respectively. Figure 2.10(b) shows the topography of the film to be uniform and homogeneous with a height of about 2 nm with reference to the substrate [19]. The topography of the film transferred at 45 mN/m at the collapsed state showed domains of different heights (Figure 2.10(c)). The AFM topography images of monolayer film of PyTp transferred at 5, 35 and 45 mN/m also showed similar features.

AFM images of the LB films of PyTp with two layers transferred onto hydrophobic silicon

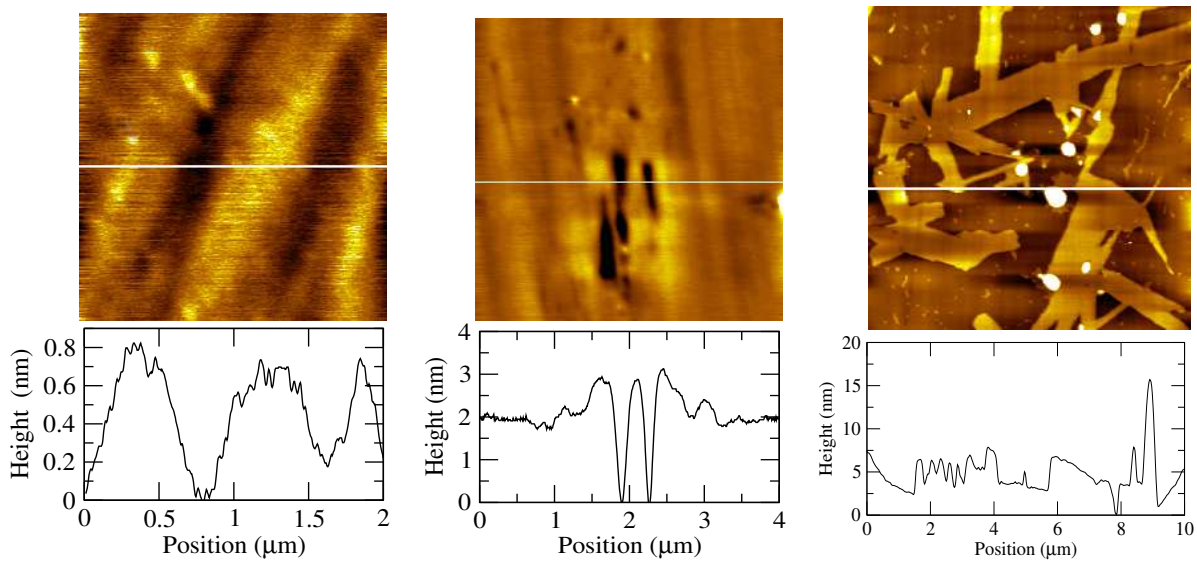

(a) (b) (c)

Figure 2.10: (a) AFM topography of ImTp monolayer transferred by horizontal method onto hydrophilic silicon substrate at a target surface pressure (π_t) of 5 mN/m. Topographies of ImTp monolayer transferred by LB technique onto hydrophilic silicon substrates at (b) π_t = 35 mN/m, and (c) π_t = 45 mN/m. The respective height profiles corresponding to the lines drawn on the images are shown below.

substrates at various target surface pressures (π_t) are shown in Figure 2.11. For the films transferred at π_t of 25 mN/m and 30 mN/m, irregular-shaped domains with significantly low surface coverage (45%) were observed (Figures 2.11(a) and 2.11(b)). However, the films transferred at π_t of 35 mN/m (Figure 2.11(c)), 38.5 mN/m (Figure 2.11(d)) and 42 mN/m (Figure 2.11(e)) revealed a much higher surface coverage (75%) with narrow rectangular voids elongated in the dipping direction of the LB deposition process. At all these surface pressures, the height profiles of the images yield a value of about 4.0±0.2 nm. The film transferred at the onset of collapse state showed a broken film structure (Figure 2.11(f)).

The narrow rectangular voids observed for the LB film of PyTp with 2 layers at 35 mN/m were further imaged at smaller scan ranges. Figures 2.12(a) and 2.12(b) show different scan ranges for the pattern with narrow rectangular voids. These voids were found to have width in the range of 80-100 nm and length in the range of 250-400 nm. These were uniformly distributed over the entire region of the film. We find consistency in the scaling of the void shapes and sizes with different scan ranges. We also find that the number of voids decreased and the film became more compact

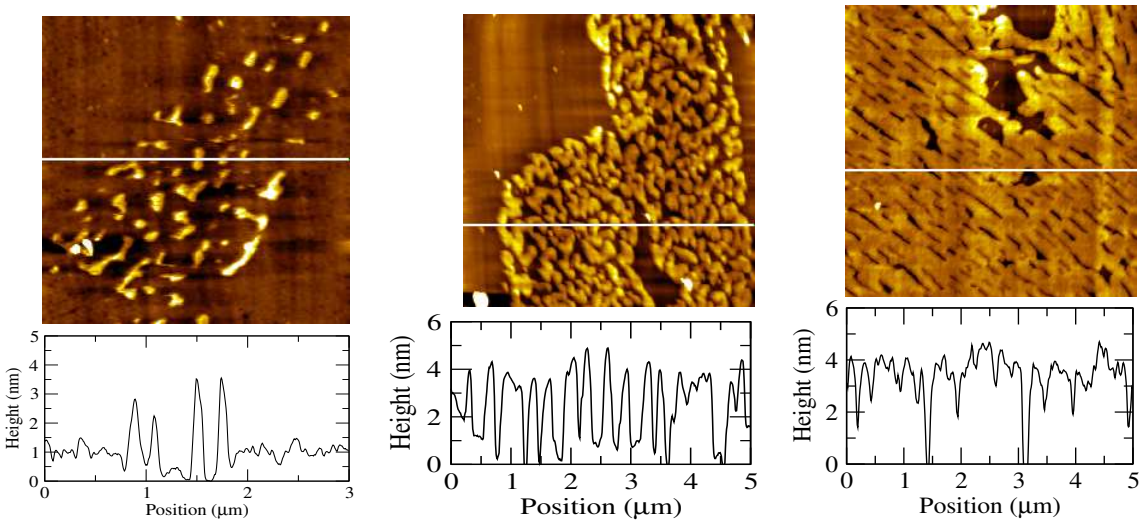

(a) π_t = 25 mN/m (b) π_t = 30 mN/m (c) π_t = 35 mN/m

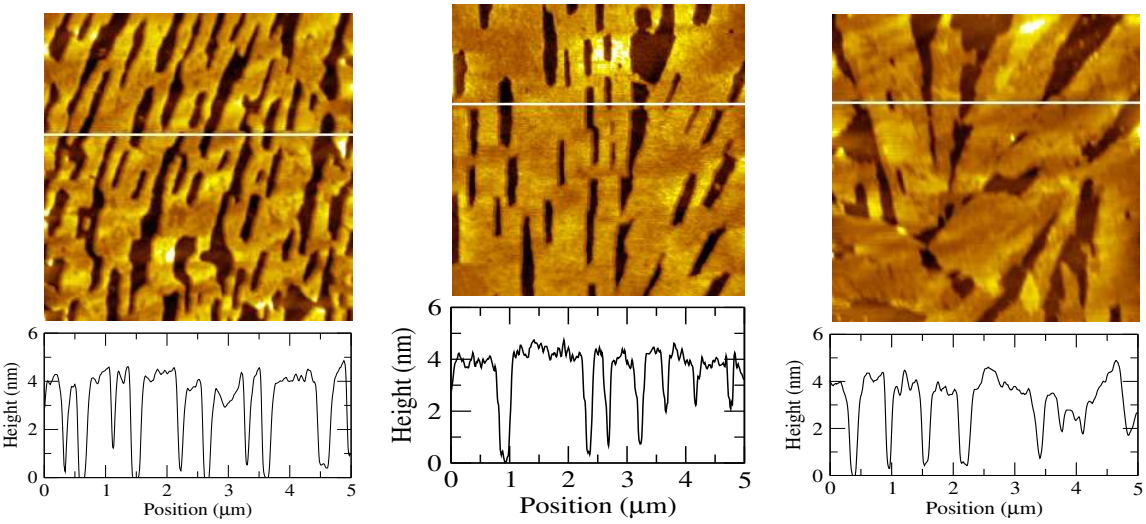

(d) π_t = 38.5 mN/m (e) π_t = 42 mN/m (f) π_t = 43.5 mN/m

Figure 2.11: AFM topography images of LB films of PyTp with two layers on hydrophobic silicon substrate transferred at different target surface pressures (π_t). The respective height profiles corresponding to the lines drawn on the images are shown below.

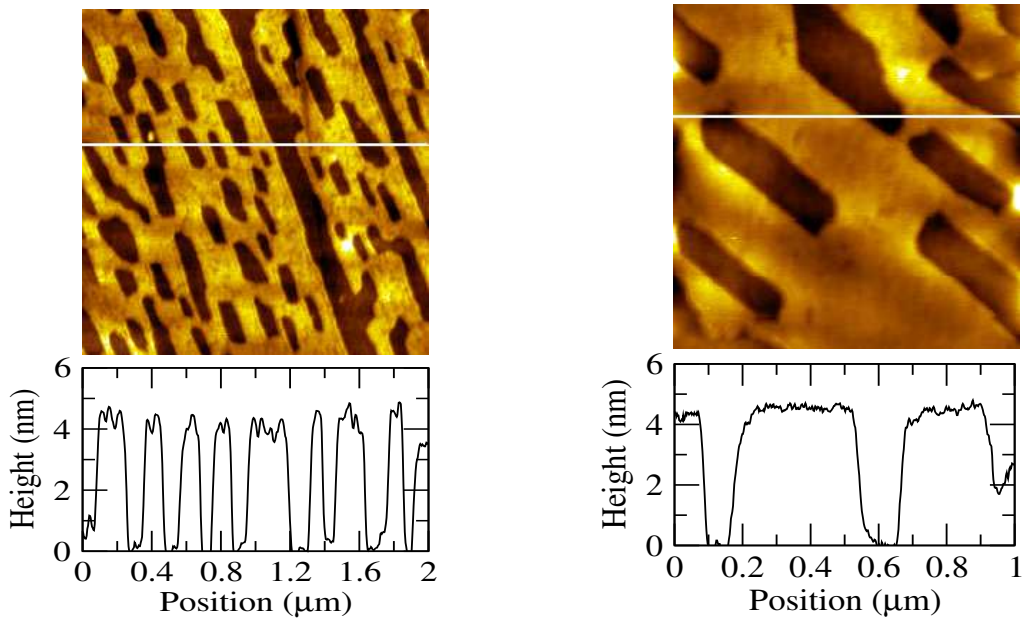

(a) 2×2 μm^2 (b) 1×1 μm^2

Figure 2.12: The uniformly distributed rectangular voids observed for the LB films of PyTp with two layers on hydrophobic silicon substrate at π_t = 35 mN/m are shown for different scan ranges. The respective height profiles corresponding to the lines drawn on the images are shown below.

with increase in π. However, full coverage could not be obtained even at a high surface pressure of 42 mN/m (Figure 2.11(e)). In addition, the topography image of PyTp film with two layers on hydrophobic glass substrate was studied to check the coverage. For a film transferred at a π_t of 35 mN/m (Figure 2.13), the coverage was found to be poor compared to the coverage obtained for the same film on hydrophobic silicon substrate. Also, the pattern with regular rectangular voids was not observed for the film on the hydrophobic glass substrate.

For the ImTp LB film with two layers transferred onto hydrophobic silicon substrates, the morphology was found to be quite different from that of the PyTp film. Figure 2.14 shows the AFM topography images of the LB film of ImTp with two layers transferred at a π_t of 35 mN/m on hydrophobic silicon substrates. The topography images showed more roughness of the film surface compared to the roughness exhibited by the PyTp film. For LB film of ImTp with two layers, the height profile showed a value of about 4.8 nm with respect to the substrate. In addition, irregular shaped voids were observed throughout the film.

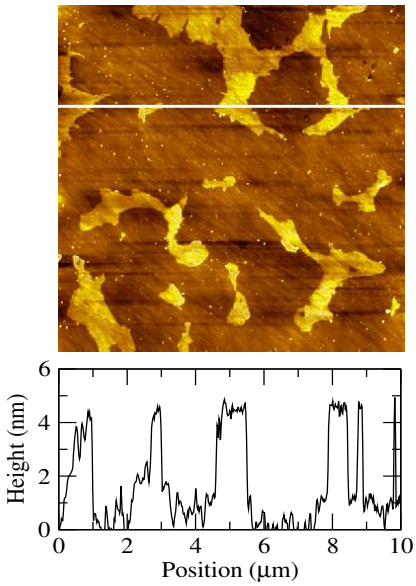

Figure 2.13: AFM topography images of LB films of PyTp with two layers transferred at π_t = 35 mN/m onto hydrophobic glass substrate. The height profile corresponding to the line drawn on the image is shown below.

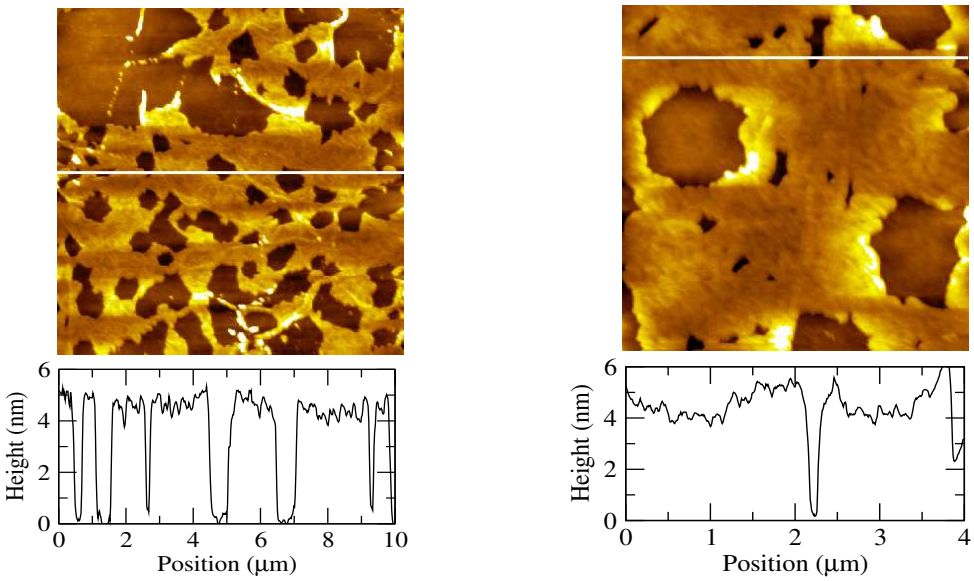

(a) $10 \times 10\ \mu m^2$ (b) $4 \times 4\ \mu m^2$

Figure 2.14: AFM topography images of LB films of ImTp with two layers on hydrophobic silicon substrate transferred at a π_t of 35 mN/m are shown for different scan ranges. The respective height profiles corresponding to the lines drawn on the images are shown below.

2.4 Discussion

The molecular structures of PyTp and ImTp are shown in Figure 2.15 with approximate dimensions according to the standard bond lengths and angles. The computed surface area of the aromatic core is equal to 0.785 nm^2 . The surface area occupied by the molecule is about 4.5 nm^2 if the extended peripheral hydrocarbon tails are included. From the π-A_m isotherms (Figures 2.3 and 2.4), we have obtained A_o values of 3.1 and 3.4 nm^2/molecule at the gradual rise region, and 1.15 and 1.40 nm^2/molecule at the steep rise region, for the PyTp and ImTp molecules respectively. Comparing these values with the molecular dimensions, we suggest that the gradual rise region is an expanded phase and the steep rise region is a condensed phase for the isotherms of both PyTp and ImTp molecules [19].

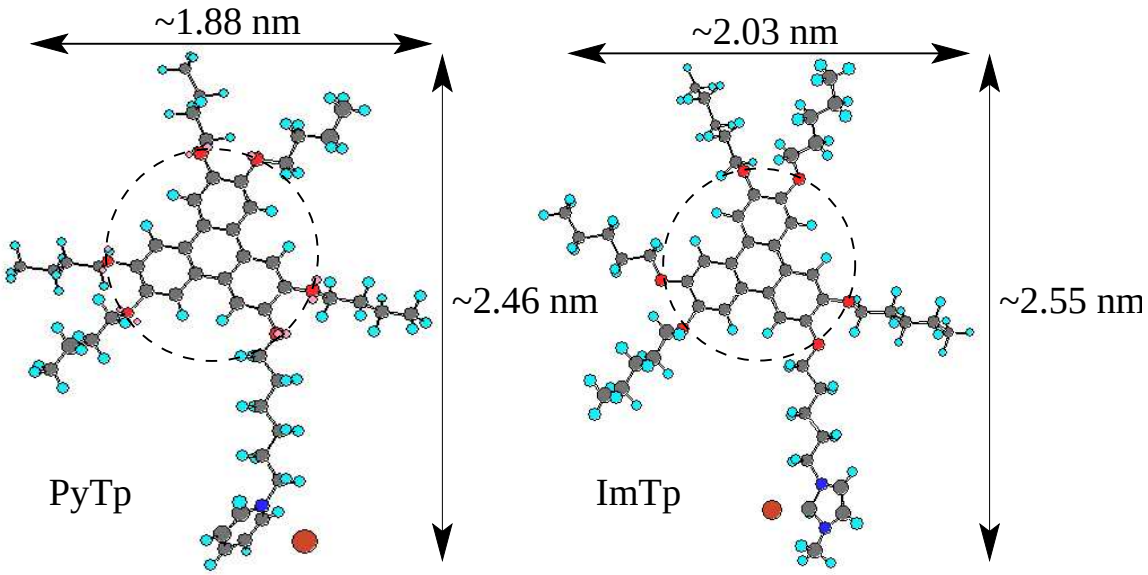

Figure 2.15: Molecular structure of PyTp and ImTp molecules with approximate dimensions according to standard bond lengths and angles. The triphenylene disc area shown in dashed circle is about 0.785 nm^2.

Additionally, the $|E|$ versus A_m plots (Figure 2.5) further confirm the phase transitions in the isotherms of PyTp and ImTp molecules. The $|E|$ values are known to characterize the nature of a monolayer's stable phases. Specifically, a maximum value of the $|E|$ in the range of 12.5 mN/m to 50 mN/m is the characteristic of a liquid expanded phase while a value between 100 to 250 mN/m is the characteristic of a liquid condensed phase [20]. The $|E|$ values calculated as a function of

A_m indicate that, for both the PyTp and ImTp systems, the monolayers undergo a phase transition from an expanded phase to a condensed phase. The maximum $|E|$ value attained by PyTp is much higher (83 mN/m) than that attained by ImTp monolayer (53.9 mN/m). This suggests that the packing of the molecules in PyTp monolayer is better than that of ImTp monolayer [19]. This may be attributed to the steric hindrance caused by an extra methyl group attached to the imidazolium nitrogen atom.

In literature, some alkoxytriphenylene derivatives have been reported [16] to form stable Langmuir monolayers with A_o value in the range 0.7 - 1.0 nm^2, but the PyTp and ImTp systems exhibit comparatively higher A_o values. This may be because of the presence of ionic groups, pyridinium and imidazolium, which tend to expand the films due to the direct electrostatic repulsion [21]. On spreading the ionic discotic molecules, the small Br^- counter-ions dissolve into the subphase due to the dissociation of the ionic groups. The presence of these Br^- counter-ions and the charged insoluble film form an ionic double layer at the interface. The rigid aromatic rings which form the core of the discotics contain delocalized Π electrons. At low area per molecule, these cores overlap due to the strong Π-Π stacking interaction, thereby forming two-dimensional analog of the columnar mesophase.

An interesting feature of the present two systems is that the monolayer on expanding and compressing shows negligible hysteresis (Figure 2.7). This indicates that the monolayer phases are reversible. Interestingly, the isotherm cycles completely revert back to its monolayer state even from the collapse state. The reversibility of the monolayer state from the collapse state was further confirmed by BAM studies (Figure 2.8). Such a system with a reversible collapse may act as an ideal model system to understand several disk-like biological systems, for example vitamins, chlorophyll and hemoglobin.

The AFM topography images (Figures 2.10(a) and 2.10(b)) showed a height of about 0.7 nm for the film transferred at 5 mN/m (expanded phase) and a height of about 2 nm for the film transferred at 35 mN/m (condensed phase). The film height of 0.7 nm corresponds to the thickness of the molecules lying parallel to the A-S interface, whereas, the film height of 2 nm corresponds to the height of the molecules lying normal to the A-S interface. On the basis of these values

of film heights and the results obtained from surface manometry, we can further infer that, at the expanded phase the molecules exhibit a face-on configuration, and at the condensed phase the molecules exhibit an edge-on configuration [19]. We schematically represent the face-on and edge-on configuration at the A-W interface as shown in Figure 2.16. In face-on configuration, the core lies flat on the water surface and the hydrocarbon tails (partially interdigited) extend away from the interface. Such a configuration may be preferred if the core of the molecule is capable of hydrogen bonding. It also maximizes the configuration space available to the aliphatic tails. In the edge-on configuration, the core lies normal to the interface with the polar end submerged in water and bottom-most tails extending roughly parallel and slightly away from the interface. Such a conformation allows the polar oxygen to be in contact with water, while minimizing water contact with the hydrophobic alkyl tails [16]. This maximizes the Π-Π interactions between the conjugated cores with the molecules arranged into columns parallel to the water surface, forming the two-dimensional analog of a columnar phase. Josefowicz et al. [1] have reported the edge-

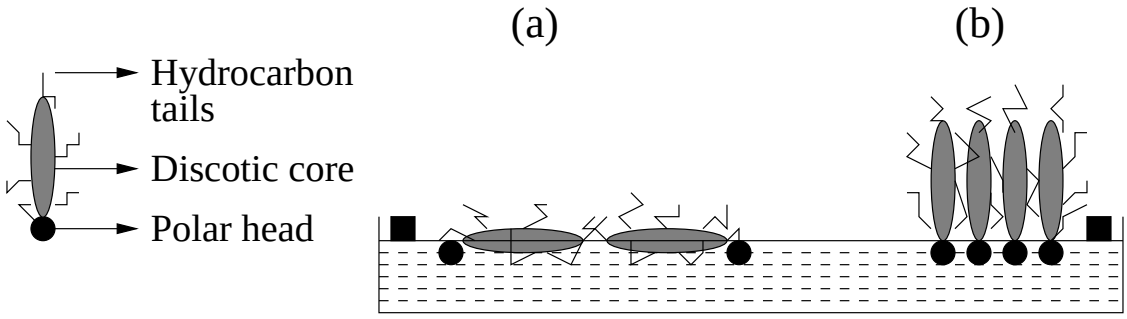

Figure 2.16: Schematic representation of (a) face-on and (b) edge-on configuration of discotic molecules at the air-water interface.

on columnar structure in the LB films of triphenylene based discotic molecules with the column alignment predominantly along the film deposition direction. However, they did not report face-on arrangement based on AFM [1]. In our system, the presence of highly polar pyridinium and imidazolium moieties together with six oxygen atoms at the periphery of the triphenylene cores have enhanced the hydrophilicity of the molecules, thereby facilitating the face-on configuration at large A_m values at the A-W interface.

We have formed LB films with 2 layers at various target surface pressures for both PyTp and ImTp, and carried out AFM imaging to study the morphology of these films (Figures 2.11 to 2.14). We observe that the surface coverage increases with increase in π_t but full coverage could not be obtained for both the films. We found that the coverage was better for both the films when they were transferred onto silicon substrates as compared to glass substrates. However, the morphology of ImTp film with two layers was markedly different from that of the morphology of PyTp film. On hydrophobic silicon substrate, the ImTp film transferred at 35 mN/m showed irregular shaped voids (Figure 2.14), whereas, on the same substrate the PyTp film transferred at the same π_t exhibited regular rectangular voids (Figure 2.12(a)).

With discotic mesogens, the effects of Π-Π and steric interactions on the molecular organization of the LB films are stronger as compared to the case of the classical rod-like molecules. UV-visible absorption spectrum taken for the LB film with two layers of PyTp yields peaks at 258, 275, 305 and 344 nm. Similar absorption peaks were also observed for the ImTp LB films with two layers. These are particularly significant, indicating Π-Π stacking interaction between the conjugated triphenylene cores.

On the basis of these observations, we suggest that the molecular organization of the ionic discotic mesogens is driven by the interaction between the substrate and the polar head (pyridinium, imidazolium) group, the steric intermolecular interactions and the strong Π-Π stacking interaction between the triphenylene cores. In addition, the molecular packing is also affected by natural dewetting of the substrate while draining or evaporation of entrapped water within the films [22–24].

2.5 Conclusions

The novel discotic mesogens, PyTp and ImTp, exhibited stable Langmuir monolayer which showed negligible hysteresis on expanding and compressing. Also, the collapsed state completely reverts to the monolayer state. As compared to the monolayers of non-ionic triphenylene derivatives reported so far, these cationic discotics showed higher limiting area per molecule due to the direct electrostatic repulsion between the molecules within the film. These monolayer films trans-

ferred at different target surface pressures by LB technique were studied employing AFM. The topography of these films, transferred at low and high surface pressure region of the isotherms, indicated a transformation of the monolayer from face-on to edge-on configuration. We find that the molecules PyTp and ImTp were arranged into columns in the bulk as seen by our x-ray studies, and two-dimensional columns at A-W and A-S interfaces as seen by our surface manometry and AFM studies.

The presence of cationic moiety in the discotic molecule opens scope for studying electrostatic interaction between such a molecule and negatively charged species like DNA at interfaces. Such an interaction may give rise to a stable complex formation with interesting properties. In the next chapter, we explore the formation of a complex of PyTp molecule with DNA at interfaces.

Bibliography

[1] J. Y. Josefowicz, N. C. Maliszewskyj, S. H. J. Idziak, P. A. Heiney, J. P. McCauley, and A. B. Smith, *Science* **260**, 323 (1993).

[2] D. Gidalevitz, O. Y. Mindyuk, P. A. Heiney, B. M. Ocko, P. Henderson, H. Ringsdorf, N. Boden, R. J. Bushby, P. S. Martin, J. Strzalka, J. P McCauley, and A. B. Smith, *J. Phys. Chem. B* **101**, 10870 (1997).

[3] A. D. Dunbar, T. M. Richardson, A. J. McNaughton, J. Hutchinson, and C. A. Hunter, *J. Phys. Chem. B* **110**, 16646 (2006).

[4] W. Pisula, A. Menon, M. Stepputat, I. Lieberwirth, U. Kolb, A. Tracz, H. Sirringhaus, T. Pakula, and K. Mullen, *Adv. Mater.* **17**, 684 (2005).

[5] J. P. Schmidtke and R. H. Friend, *J. Chem. Phys.* **124**, 174704 (2006).

[6] S. Kumar and S. K. Varshney, *Angew. Chem. Int. Ed.* **39**, 3140 (2000).

[7] M. Van der Auweraer *et al. Thin Solid Films* **210/211**, 39 (1992).

[8] N. C. Maliszewskyj, P. A. Heiney, K. J. Blasie, J. P. McCauley, and A. B. Smith, *J. Phys. II France* **2**, 75 (1992).

[9] G. Roberts, *Langmuir-Blodgett Films*, Plenum Press: New York, 1990.

[10] N. C. Maliszewskyj, P. A. Heiney, J. Y. Josefowicz, J. P. McCauley, and A. B. Smith, *Science* **264**, 77 (1994).

[11] R. Ionov and A. Angelova, *Phy. Rev. E* **52**, 21(R) (1995).

[12] S. Chandrasekhar, *Liq. Cryst.* **14**, 3 (1993).

[13] C. A. Hunter and J. K. M. Sanders, *J. Am. Chem. Soc.* **112**, 5525 (1990).

[14] K. Binnemans, *Chem. Rev.* **105**, 4148 (2005).

[15] M. Yoshio, T. Mukai, H. Ohno, and T. Kato, *J. Am. Chem. Soc.* **126**, 994 (2004).

[16] O. Y. Mindyuk and P. A. Heiney, *Adv. Mater.* **11**, 341 (1999).

[17] Sandeep Kumar and Santanu Kumar Pal, *Tetrahedron Letters* **46**, 4127 (2005).

[18] Sandeep Kumar and Santanu Kumar Pal, *Tetrahedron Letters* **46**, 2607 (2005).

[19] Alpana Nayak, K. A. Suresh, Santanu Kumar Pal, and Sandeep Kumar, *J. Phys. Chem. B* **111**, 11157 (2007).

[20] J. T. Davies and E. K. Rideal, *Interfacial Phenomena*; Academic Press: New York, 1961.

[21] G. L. Gaines Jr., *Insoluble Monolayers at Liquid Gas Interface*, Interscience: New York, (1966).

[22] G. Reiter, *Phys. Rev. Lett.* **68**, 75 (1992).

[23] H. D. Sikes, J. T. Woodward IV, and D. K. Schwartz, *J. Phys. Chem.* **100**, 9093 (1996).

[24] Raj Kumar Gupta and K. A. Suresh, *Eur. Phys. J. E* **14**, 35 (2004).